

---

# BAYESIAN OPTIMIZATION UNDER UNCERTAINTY FOR TRAINING A SCALE PARAMETER IN STOCHASTIC MODELS

---

**Akash Yadav**  
University of Houston  
ayadav4@uh.edu

**Ruda Zhang**  
University of Houston  
rudaz@uh.edu

## ABSTRACT

Hyperparameter tuning is a challenging problem especially when the system itself involves uncertainty. Due to noisy function evaluations, optimization under uncertainty can be computationally expensive. In this paper, we present a novel Bayesian optimization framework tailored for hyperparameter tuning under uncertainty, with a focus on optimizing a scale- or precision-type parameter in stochastic models. The proposed method employs a statistical surrogate for the underlying random variable, enabling analytical evaluation of the expectation operator. Moreover, we derive a closed-form expression for the optimizer of the random acquisition function, which significantly reduces computational cost per iteration. Compared with a conventional one-dimensional Monte Carlo-based optimization scheme, the proposed approach requires 40 times fewer data points, resulting in up to a 40-fold reduction in computational cost. We demonstrate the effectiveness of the proposed method through two numerical examples in computational engineering.

**Keywords** optimization under uncertainty · stochastic models · hyperparameter tuning · scale · precision · Bayesian optimization · Bayesian generalized linear model

## 1 Introduction

Optimization under uncertainty is a fundamental challenge in decision-making, arising whenever system parameters or states are uncertain and need to be modeled as random variables or stochastic processes. Such problems appear across diverse domains, including process scheduling and planning (Li and Ierapetritou, 2008; Verderame et al., 2010), system operations (Zhang and Ghanem, 2020, 2022), hazard management (Zhang et al., 2020) and engineering design (Agarwal and Renaud, 2004; Agarwal et al., 2004). Over the years, several approaches have been developed to address problems of this nature.

Stochastic programming (Dantzig, 1955; Birge and Louveaux, 2011) is one of the earliest formal frameworks for optimization under uncertainty, and a detailed survey of its applications to process systems is given in Li and Grossmann (2021). Robust optimization, introduced by Bai et al. (1997) and later applied to truss topology design (Ben-Tal and Nemirovski, 1997), has since been substantially advanced (Ben-Tal and Nemirovski, 2002; Bertsimas et al., 2011), with a

comprehensive review available in [Beyer and Sendhoff \(2007\)](#). Chance-constrained optimization, first formulated by [Charnes and Cooper \(1959\)](#) for temporal planning problems, has also seen extensive development ([Miller and Wagner, 1965](#); [Nemirovski and Shapiro, 2007](#)) and applications across finance, engineering, and operations research. Simulation-based optimization is an active area within stochastic optimization. Comprehensive reviews of its developments are available in [Carson and Maria \(1997\)](#) and [Andradottir \(1998\)](#), while simulation-based design under uncertainty is surveyed in the special issue by [Li et al. \(2016\)](#).

Bayesian optimization has emerged as a powerful tool for global optimization of expensive black-box functions, particularly in machine learning contexts such as hyperparameter tuning ([Snoek et al., 2012](#); [Bergstra et al., 2011](#)) and neural architecture search ([White et al., 2021](#)). [Turner et al. \(2021\)](#) showed that Bayesian optimization can achieve better performance than random search in hyperparameter tuning for machine learning. More recently, it has been adapted for optimization under uncertainty ([Beland and Nair, 2017](#); [Oliveira et al., 2019](#); [Yang et al., 2023](#)), with multifidelity approaches surveyed in [Do and Zhang \(2025\)](#) and [Zhang and Alemazkour \(2024\)](#). These advances broaden the applicability of Bayesian optimization and motivate its use in more specialized problems.

In this work, we are interested in a specific problem, i.e., the optimization of a scale- or precision-type parameter in stochastic models. A *scale parameter* of a probability measure controls how spread out the distribution is around its central value; depending on context, it may be referred to as variance, dispersion, bandwidth, or temperature. Conversely, a *precision* (or *concentration*) *parameter* controls how tightly the distribution clusters around the central value. Scale and precision parameters are connected by monotone transforms (e.g., precision = 1 / variance) and can be treated in a unified framework. Accurate optimization of such parameters is essential for sharp and reliable uncertainty quantification. However, because the system under study is stochastic and often complex and high-dimensional, tuning such hyperparameters becomes a challenging problem of optimization under uncertainty.

This problem is motivated by the authors' recent work on model error characterization using a stochastic reduced-order modeling framework ([Yadav and Zhang, 2025](#)). The stochastic subspace model therein contains a hyperparameter, denoted by  $\beta$ , which controls the spread of the distribution. The optimization approach adopted in [Yadav and Zhang \(2025\)](#) estimated the expectation using Monte Carlo sample averages and then optimized the estimated objective function with a one-dimensional optimization algorithm such as golden section search and successive parabolic interpolation. This strategy suffers from two limitations: (i) Monte Carlo estimates of the expectation operator are noisy and fail to exploit global structure in the objective function, and (ii) data inefficiency becomes severe when pointwise noise dominates the underlying function variability. Related stochastic reduced-order modeling approaches ([Soize and Farhat, 2017](#); [Wang et al., 2019](#); [Azzi et al., 2022](#)) often rely on trial-and-error with large numbers of Monte Carlo samples, which exacerbates the same inefficiency.

To overcome these limitations, we introduce a novel Bayesian optimization framework that addresses optimization under uncertainty with significantly improved data efficiency. We demonstrate its effectiveness in optimizing a scale / precision parameter in stochastic models. Our main contributions are:

1. Development of a statistical surrogate for the objective function, enabling analytical evaluation of the expectation operator without Monte Carlo sampling.

2. Derivation of a closed-form solution for the optimum of the random acquisition function, enabling efficient selection of new observation points and reducing per-iteration computational cost.
3. Validation through numerical experiments, showing that the proposed method achieves up to a 40-fold improvement in both data usage and computational cost, making it suitable for real-time prediction tasks.

The remainder of the paper is organized as follows. [Section 2](#) introduces the optimization under uncertainty problem. [Section 3](#) presents the proposed Bayesian optimization framework. [Section 4](#) describes its application to optimizing a concentration parameter in stochastic models. Numerical results are reported in [Section 5](#), followed by discussion in [Section 6](#) and concluding remarks in [Section 7](#).

## 2 Problem statement

We consider the problem of optimizing a scale- or precision-type parameter  $\beta > 0$  in the presence of uncertainty, formulated as:

$$\min_{\beta \in (0, \infty)} \mathbb{E}[g(s(\boldsymbol{\omega})) | \beta], \quad (1)$$

where  $\boldsymbol{\omega}$  is a (potentially high-dimensional) random variable,  $s(\boldsymbol{\omega}) \geq 0$  is a summary statistic and  $g(\cdot)$  is a known function. The hyperparameter  $\beta$  controls the spread of the distribution of  $\boldsymbol{\omega}$ , such that increasing  $\beta$  increases variability in the statistic; or inversely, it controls the concentration of the distribution of  $\boldsymbol{\omega}$ , such that increasing  $\beta$  reduces variability in the statistic.

The formulation in [Eq. \(1\)](#) is intentionally kept broad: different problems may encounter different choices of the function  $g(\cdot)$ . In this work, we focus on the case where  $g(x) = |x - s_0|^2$ , where  $s_0$  is a target statistic against which  $s(\boldsymbol{\omega})$  is compared. However, the proposed methodology is not limited to this setting and can be adapted to other forms of  $g$ . Under this choice, the optimization problem becomes:

$$f_{\text{true}}(\beta) := \mathbb{E}[|s(\boldsymbol{\omega}) - s_0|^2 | \beta], \quad (2)$$

with the optimal hyperparameter

$$\beta_{\text{true}}^* := \arg \min_{\beta \in (0, \infty)} f_{\text{true}}(\beta). \quad (3)$$

## 3 Methodology

The main challenge in solving this optimization under uncertainty problem is the inaccessible expectation operator. While it can be approximated using Monte Carlo sample averages, high variability in the random variable  $\boldsymbol{\omega}$  demands large sample sizes for accurate approximation. As a result, the approach requires a large number of function evaluations, which can be computationally expensive. To address this challenge, we propose a Bayesian optimization (BO) approach that is substantially more data-efficient than the Monte Carlo approach. While BO methods are known to be data-efficient and well-suited for expensive-to-evaluate objective functions, the novelty of our approach lies in designing a BO method that is tailored for optimization under uncertainty. The core idea is to construct a statistical surrogate for the random variable  $s(\boldsymbol{\omega})$  conditioned on  $\beta$ , so that the expectation in the objective function  $f_{\text{true}}(\beta)$  can be computed analytically. Due to the structure of the surrogate, a further advantage of this BO approach is that the derived surrogate for the objective function can be optimized analytically.

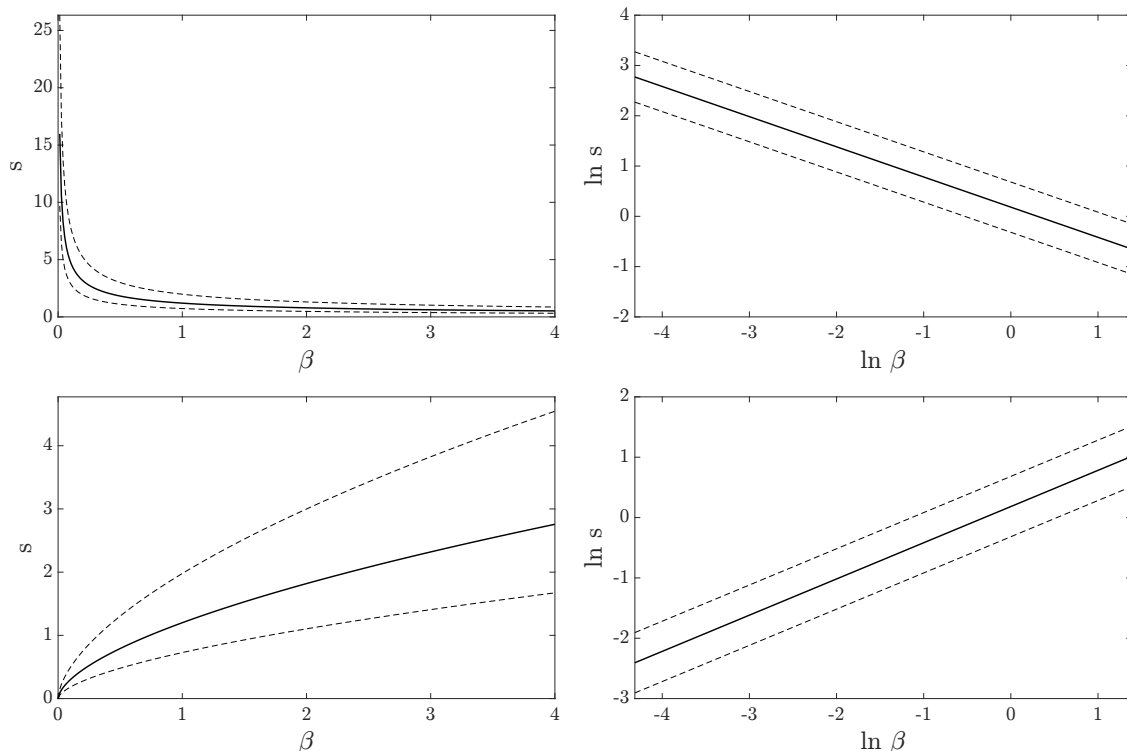


Figure 1: Conditional model of  $s|\beta$ . The left panel shows the mean of  $s$  as a power function of  $\beta$  for positive and negative exponents, with dashed curves indicating the 2.5th and 97.5th conditional percentiles. The right panel presents the corresponding log–log transformations ( $\ln s$  vs.  $\ln \beta$ ), where the relationship is linear.

### 3.1 Assumption

A key structural assumption in this work is that the expectation of the statistic scales approximately as a power law (see Fig. 1):

$$\mathbb{E}[s(\omega)|\beta] \propto \beta^a. \quad (4)$$

This assumption is consistent with many statistical settings. A classical example is when  $\omega = (x_1, \dots, x_n)$  is a random sample, the scale parameter  $\beta$  is the variance  $\sigma^2$  of the population, and the statistic  $s(\omega) = |\bar{x} - \mathbb{E}[x]|^2$  is the squared error of the sample mean  $\bar{x} = \frac{1}{n} \sum_{i=1}^n x_i$ . In this setting, reducing  $\beta$  (i.e., lower variance or, equivalently, higher precision) reduces the variability of the sample mean, and the statistic vanishes as  $\beta$  tends to zero. The expectation of the statistic is exactly linear in the scale parameter:  $\mathbb{E}[s(\omega)|\beta] = \frac{1}{n} \sigma^2$ . This relation changes under different parameterizations (e.g., standard deviation  $\sigma$  or precision  $\sigma^{-2}$ ), but remains a power law with various exponents (e.g., 2 or -1). Another example is when we take the parameter  $\beta$  in the previous example to be sample size  $n$  instead. From the central limit theorems, we know that sample mean  $\bar{x}$  converges to population mean  $\mathbb{E}[x]$  at a polynomial rate of  $-\frac{1}{2}$ , as sample size  $n$  tends to infinity. Therefore we have  $\mathbb{E}[s(\omega)|\beta] \propto n^{-1}$  asymptotically. More broadly, the assumption in Eq. (4) often applies when the summary statistic  $s(\omega)$  involves averaging over weakly correlated random variables, such as the Euclidean norm and other vector  $p$ -norms.

### 3.2 Surrogate modeling

A central idea of the proposed method is to build a probabilistic surrogate for the statistic  $s(\boldsymbol{\omega})$  conditioned on the scale or precision parameter  $\beta$ , exploiting its approximate power-law scaling. Consider the classical example in the previous subsection as a prototype. For a Gaussian random variable  $x \sim N(\mu, \sigma^2)$ , we know that the sample mean  $\bar{x} \sim N(\mu, \sigma^2/n)$ . In other words,  $\bar{x} = \mu + \frac{\sigma}{\sqrt{n}}z$  where  $z \sim N(0, 1)$ . Therefore we can write:

$$\ln |\bar{x} - \mu| = -\frac{1}{2} \ln n + \frac{1}{2} \ln \sigma^2 + \ln |z|. \quad (5)$$

Based on this, we propose a conditional statistical model for  $s(\boldsymbol{\omega})$  given  $\beta$  in the form of a Bayesian generalized linear model (GLM):

$$\ln s(\boldsymbol{\omega}) = a \ln \beta + \ln b + \varepsilon z, \quad z \sim N(0, 1), \quad (6)$$

where  $a$  is the exponent of the power law,  $b$  is a scaling parameter, and  $\varepsilon$  captures variability around the power-law trend. Here we adopt an independent Gaussian noise  $z \sim N(0, 1)$  for analytical tractability; alternative noise models are discussed in [Section 6](#). For simplicity, we use the standard noninformative prior for the GLM parameters  $(a, \ln b, \varepsilon)$ . Denote coefficients  $\boldsymbol{\theta} = (a, \ln b)$ , the standard noninformative prior is uniform on  $(\boldsymbol{\theta}, \ln \varepsilon^2)$  and has an improper distribution:  $p(\boldsymbol{\theta}, \varepsilon^2) \propto \varepsilon^{-2}$ . The distribution is improper because it has an infinite integral over its domain  $\mathbb{R}^2 \times (0, \infty)$ .

Notice that, with the surrogate model described above, the random variable that drives the uncertainty in  $s$  reduces from the potentially high-dimensional  $\boldsymbol{\omega}$  to a four-dimensional one:  $(\boldsymbol{\theta}, \varepsilon^2, z)$ . Such a simplification in uncertainty representation is acceptable, as we only seek to approximate the moments of  $s$  given  $\beta$ .

*Inference.* For the GLM in [Eq. \(6\)](#), denote input  $\mathbf{x} = (\ln \beta, 1)$  and output  $y = \ln s(\boldsymbol{\omega})$ . Given a dataset  $\mathcal{D} = \{(\mathbf{x}^i, y^i)\}_{i=1}^n$  with an input sample  $\mathbf{X} = [\mathbf{x}^1 \cdots \mathbf{x}^n]^\top \in \mathbb{R}^{n \times k}$  and output observations  $\mathbf{y} = (y^1, \dots, y^n)$ , the classical estimates of the GLM parameters  $(\boldsymbol{\theta}, \varepsilon^2)$  are:

$$\hat{\boldsymbol{\theta}} = \mathbf{X}^\dagger \mathbf{y}, \quad s^2 = \frac{1}{n-k} \hat{\mathbf{r}}^\top \hat{\mathbf{r}}, \quad (7)$$

where  $\dagger$  denotes the Moore–Penrose inverse and  $\hat{\mathbf{r}} = \mathbf{y} - \mathbf{X}\hat{\boldsymbol{\theta}}$  is the residual. If  $\mathbf{X}$  has full column rank, then  $\mathbf{X}^\dagger = (\mathbf{X}^\top \mathbf{X})^{-1} \mathbf{X}^\top$ . With the standard noninformative prior, the posterior distribution of the GLM parameters can be written as:

$$\varepsilon^2 | \mathcal{D} \sim \text{Inv-}\chi^2(n-k, s^2), \quad \boldsymbol{\theta} | \varepsilon^2, \mathcal{D} \sim N(\hat{\boldsymbol{\theta}}, \varepsilon^2 \mathbf{V}_\theta), \quad (8)$$

where  $\mathbf{V}_\theta = (\mathbf{X}^\top \mathbf{X})^{-1}$ . The scaled inverse chi-squared distribution  $\text{Inv-}\chi^2(\nu, s^2)$  is the distribution of  $\nu s^2/x$  where  $x \sim \chi^2(\nu)$  is a chi-squared random variable with  $\nu$  degrees of freedom. For any input sample  $\tilde{\mathbf{X}} = [\tilde{\mathbf{x}}^1 \cdots \tilde{\mathbf{x}}^m]^\top \in \mathbb{R}^{m \times k}$ , the Bayesian GLM gives a prediction  $\tilde{\mathbf{y}} = (\tilde{y}^1, \dots, \tilde{y}^m)$  with the joint distribution:

$$\tilde{\mathbf{y}} | \mathcal{D} \sim t_m(\tilde{\mathbf{X}}\hat{\boldsymbol{\theta}}, s^2(\mathbf{I}_m + \tilde{\mathbf{X}}\mathbf{V}_\theta\tilde{\mathbf{X}}^\top), n-k), \quad (9)$$

where  $t_m(\boldsymbol{\mu}, \boldsymbol{\Sigma}, \nu)$  is the  $m$ -dimensional  $t$ -distribution with mean  $\boldsymbol{\mu}$ , covariance  $\boldsymbol{\Sigma}$ , and degrees of freedom  $\nu$ . [Figure 2](#) shows the GLM fit using a large number of data points and a Bayesian GLM fit during the Bayesian optimization process. We can observe that both GLM and Bayesian GLM are

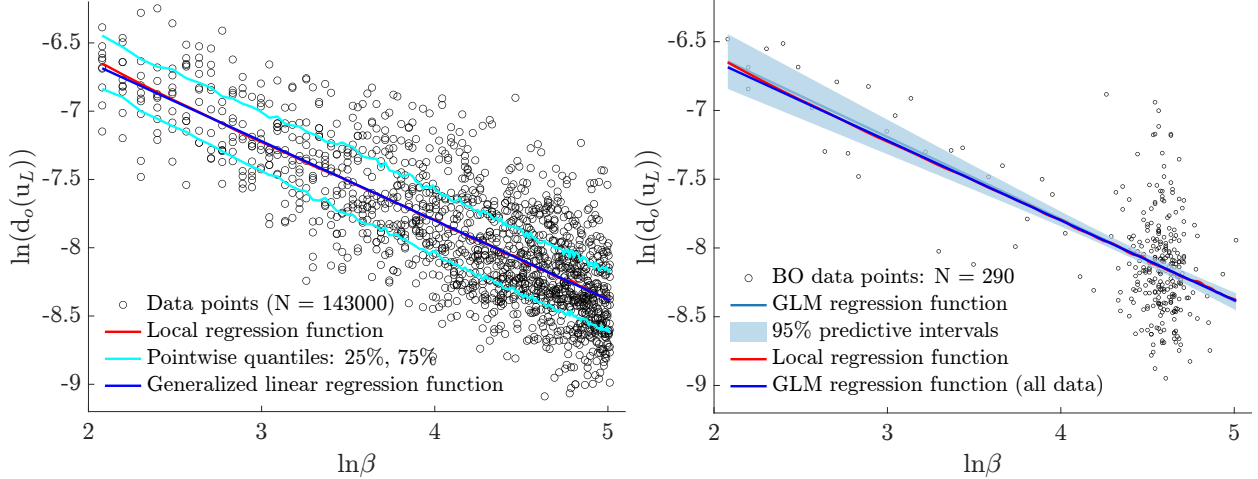


Figure 2: Static problem: raw data and surrogate model fit. (Left) Raw data is highly noisy with a downward linear trend. Plotted points are 1% of the data, uniformly subsampled. (Right) Bayesian GLM constructed during Bayesian optimization captures the GLM regression function accurately with quantified error, using much fewer data points.

able to capture the downward trend of the data. The data used here comes from the static problem described in [Section 5.1](#).

The Bayesian GLM also induces a surrogate model on the objective function. From [Eq. \(6\)](#), the conditional model can be written as:

$$s(\boldsymbol{\omega})|\beta = b\beta^a\zeta, \quad \zeta = \exp(\varepsilon z) \sim \ln N(0, \varepsilon^2). \quad (10)$$

Here  $\zeta$  has a log-normal distribution  $\ln N(0, \varepsilon^2)$  because  $\ln \zeta = \varepsilon z \sim N(0, \varepsilon^2)$ , with mean  $\mathbb{E}[\zeta] = \exp(\frac{1}{2}\varepsilon^2)$  and variance  $\mathbb{V}[\zeta] = \exp(2\varepsilon^2) - \exp(\varepsilon^2)$ . Plugging the conditional model into [Eq. \(2\)](#), we obtain a surrogate model of the objective function:

$$\begin{aligned} f(\beta) &= \mathbb{E}[|b\beta^a\zeta - s_0|^2] = \mathbb{V}[b\beta^a\zeta] + (\mathbb{E}[b\beta^a\zeta] - s_0)^2 = b^2\beta^{2a}\mathbb{V}[\zeta] + (b\beta^a\mathbb{E}[\zeta] - s_0)^2 \\ &= b^2\beta^{2a} [\exp(2\varepsilon^2) - \exp(\varepsilon^2)] + [b\beta^a \exp(\frac{1}{2}\varepsilon^2) - s_0]^2. \end{aligned} \quad (11)$$

Here, the expectation is taken with respect to  $z$ . Along with the posterior distribution of the GLM parameters in [Eq. \(8\)](#), this gives a probabilistic surrogate of the objective function. We may also plug in the classical GLM estimate in [Eq. \(7\)](#) to obtain a deterministic surrogate of the objective function.

*Discussion.* Typical BO methods construct a probabilistic surrogate for the objective function directly, and most of the time the surrogate is a generic Gaussian process ([Do et al., 2024b](#)). Our proposed approach exploits the analytical form of the objective function, and builds a probabilistic surrogate for a component random variable instead. The Bayesian GLM for the random variable induces a parametric non-Gaussian random process as a probabilistic surrogate for the objective function.

### 3.3 Acquisition function

Once a probabilistic surrogate is constructed given the available data, a BO algorithm selects the next observation location, evaluates the objective function, and then updates the surrogate with the

new data point. The process iterates until the optimization is terminated. At each iteration, the new observation location is identified as the global optimum of an acquisition function, which is derived from the probabilistic surrogate.

In this work, the probabilistic surrogate  $f(\beta)$  in Eq. (11) is a complex transform of the GLM parameters  $(\theta, \varepsilon^2)$ , so it is difficult to conduct inference analytically. This creates a challenge in using many common acquisition functions for BO, which requires computing the mean, variance, or other expectations of the surrogate. But since it is straightforward to sample  $f(\beta)$ , we choose *Thompson sampling* as the acquisition strategy: a posterior sample of the objective function is used as the acquisition function, whose global optimum is used as the next observation location. In our case, a posterior sample of the GLM parameters can be sampled via Eq. (8), which is then plugged into Eq. (11) to obtain a posterior sample of the objective function.

*Discussion.* For BO with a continuous design space, Thompson sampling is implemented in various ways, including pointwise joint sampling and spectral sampling. Do et al. (2025) gives a detailed presentation of various approaches to sampling from Gaussian process posterior. Pointwise joint sampling creates exact samples on a finite set of design points, by sampling from the joint distribution of the objective function values at those points. This method becomes prohibitively costly as the number of sample points increases.

Spectral sampling creates approximate samples throughout the entire design space, based on a representation of the objective function. The representation could be a linear combination of basis functions, such as the kernel eigenfunctions or the Fourier basis. Such a representation is usually an infinite series, and in practice only the coefficients of the leading terms are sampled, which defines an approximate sample of the objective function. In comparison, our proposed approach creates exact function samples, thanks to the parametric structure of the surrogate model.

Posterior samples can be used for the Monte Carlo approximation of many acquisition functions, bypassing the need for analytic inference. Sample average approximation also provides a way to control the exploration–exploitation tradeoff in Thompson sampling (Do et al., 2024a). Here we stick with the classic Thompson sampling for its simplicity and analytic advantage further detailed below.

### 3.4 Global optimization

Usually, the global optimization of acquisition functions in BO methods depends on numerical optimization algorithms. Specialized algorithms are often needed for accurate and scalable optimization, especially for Thompson sampling (Adebiyi et al., 2025). But for the BO method we are proposing, the acquisition functions are the posterior sample function given in Eq. (11), whose global minimum has an analytical solution.

The derivative of the posterior sample function can be written as:

$$f'(\beta) = b^2 [\exp(2\varepsilon^2) - \exp(\varepsilon^2)] (2a\beta^{2a-1}) + 2 [b \exp(\frac{1}{2}\varepsilon^2) \beta^a - s_0] [b \exp(\frac{1}{2}\varepsilon^2) (a\beta^{a-1})].$$

Let  $C_1 = b^2 [\exp(2\varepsilon^2) - \exp(\varepsilon^2)]$  and  $C_2 = b \exp(\frac{1}{2}\varepsilon^2)$ , then we have:

$$f'(\beta) = 2a\beta^{a-1}[C_1\beta^a + (C_2\beta^a - s_0)C_2].$$

We see that the critical point condition  $f'(\beta_0) = 0$  is equivalent to  $\beta_0^a = s_0 C_2 / (C_1 + C_2^2)$ . Since there is only one critical point for  $\beta \in (0, \infty)$ , it is the only internal extremum of  $f(\beta)$ . Further

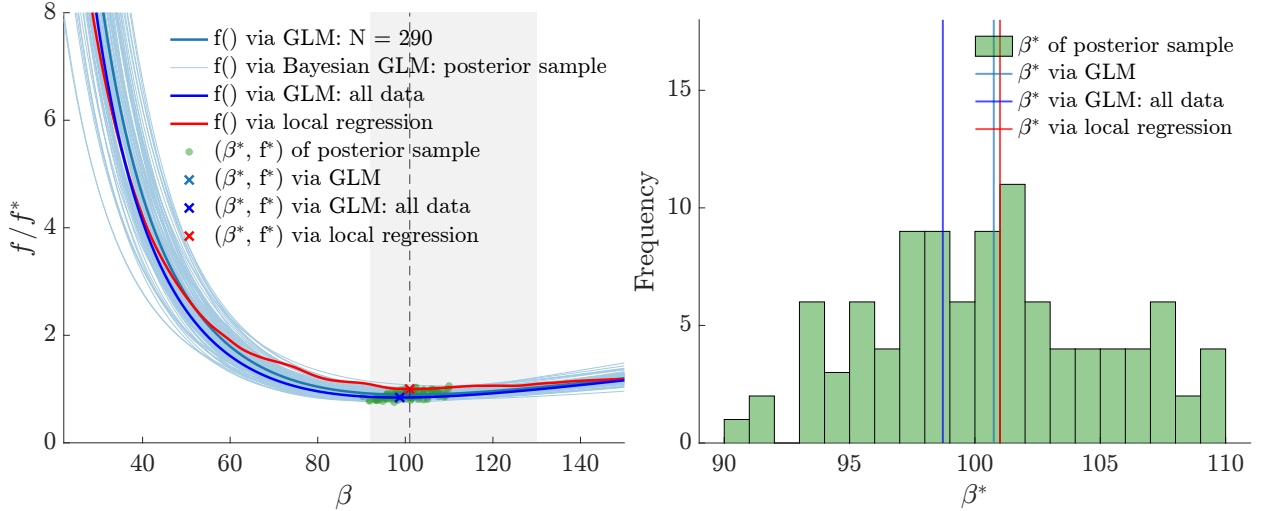


Figure 3: Static problem: optimization results under different approaches. (Left) Posterior distribution of  $(\beta^*, f^*)$  well captures the true statistics. (Right) Histogram of  $\beta^*$  posterior samples.

examination shows that  $f'(\beta) < 0$  for  $\beta < \beta_0$  and  $f'(\beta) > 0$  for  $\beta > \beta_0$ , which means that  $\beta_0$  is the global minimum of  $f(\beta)$ . Therefore, we can write:

$$\beta^* := \arg \min_{\beta \in (0, \infty)} f(\beta) = \left( \frac{s_0}{b \exp(\frac{3}{2}\varepsilon^2)} \right)^{1/a}. \quad (12)$$

Given a posterior sample of  $(a, b, \varepsilon^2) | \mathcal{D}$  via Eq. (8), the above formula gives a posterior sample of  $\beta^* | \mathcal{D}$ , which is our current probabilistic estimate of the optimal hyperparameter  $\beta_{\text{true}}$ . Plugging in the classical GLM estimate in Eq. (7) gives a deterministic estimate of  $\beta_{\text{true}}$ . Figure 3 shows some posterior samples of  $f(\beta)$  at an iteration during the BO process, as well as the corresponding Thompson samples  $(\beta^*, f^*)$ , where  $f^* := f(\beta^*)$ .

### 3.5 Observation mode

While optimization is fundamentally a sequence of decisions, parallelization can sometimes be exploited to accelerate data acquisition. For example, if the objective function is approximated via Monte Carlo sampling, the sampling process can be parallelized trivially. To enable parallelization in the proposed BO approach, we use a synchronous batch policy: at each iteration, a batch of observation locations are designed and observations are obtained, before designing the next batch of observation locations.

For Thompson sampling, it is straightforward to design a batch of observation locations: simply generate multiple samples of  $\beta^* | \mathcal{D}$ . Figure 4 shows the sequence of sample points during BO iterations, where after an initial sample of size 40, uniform in  $\ln \beta$ , we use a batch size of 10 for Thompson sampling. The figure also shows the evolution of the posterior distribution  $\beta^* | \mathcal{D}$  and the GLM estimate.

## 4 Application: Concentration parameter optimization in stochastic models

We now apply the proposed framework to the optimization of a concentration parameter in stochastic models.

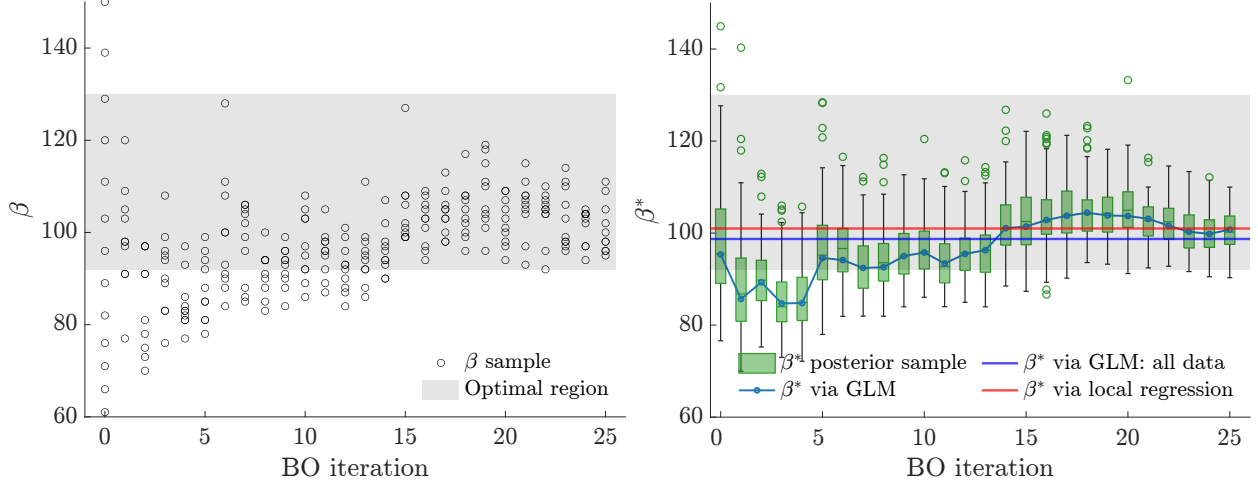


Figure 4: Static problem: progression of Bayesian optimization. (Left) Sample points during BO iterations. (Right) Evolution of  $\beta^*$  posterior distribution and GLM estimate.

Let  $F^o(\mathbf{a})$  denotes a reference model with input  $\mathbf{a}$ . Let  $F_L(\mathbf{a}; \mathcal{V})$  be the low-fidelity, reduced-order model (ROM) on a subspace  $\mathcal{V}$ , and let  $\mathcal{W}$  be a stochastic subspace with a concentration parameter  $\beta$ . To characterize the predictive error of the reference model using a stochastic reduced-order model (SROM)  $F_L(\mathbf{a}; \mathcal{W})$ , we train the concentration parameter so that the experimental validation data  $\mathbf{u}_E$  behaves like a typical SROM prediction. Specifically, denote the  $L^2$  distance of an output to a reference prediction  $\mathbf{u}^o$  as:

$$d_o(\mathbf{u}) = \|\mathbf{u} - \mathbf{u}^o\|_{L^2}. \quad (13)$$

The functional  $d_o$  summarizes the SROM prediction  $\mathbf{u}_L = F_L(\mathbf{a}; \mathcal{W})$ , a random process, into a random variable  $d_o(\mathbf{u}_L)$  which characterizes the variability of  $\mathbf{u}_L$ . The objective function for the hyperparameter  $\beta$  is then defined as the mean squared error of  $d_o(\mathbf{u}_L)$  from  $d_o(\mathbf{u}_E)$ , that is:

$$f_{\text{true}}(\beta) := \mathbb{E}[|d_o(\mathbf{u}_L) - d_o(\mathbf{u}_E)|^2 | \beta]. \quad (14)$$

This is a direct instance of the abstract problem in Eqs. (1) and (2), where random variable  $\omega = \mathcal{W}$ , summary statistic  $s(\omega) = \|F_L(\mathbf{a}; \omega) - \mathbf{u}^o\|_{L^2}$ , and function  $g(x) = |x - d_o(\mathbf{u}_E)|^2$ . The optimal hyperparameter is defined as:

$$\beta_{\text{true}}^* := \arg \min_{\beta \in [k, \infty)} f_{\text{true}}(\beta). \quad (15)$$

This formulation casts hyperparameter tuning in SROMs as an optimization-under-uncertainty problem, making it directly amenable to the Bayesian optimization framework developed in Section 3. We now summarize the steps for implementing the proposed approach for optimizing the concentration parameter in stochastic models.

1. **Input:** Bounds  $[\beta_{\min}, \beta_{\max}]$ , initial design size  $n_0$ , batch size  $B$ , maximum iterations  $T$ .
2. **Initialize sampling:** Select  $n_0$  initial values of  $\beta$ , uniformly in log scale over  $[\ln \beta_{\min}, \ln \beta_{\max}]$  and evaluate the SROM at these values to obtain an initial dataset  $\mathcal{D}_0$ . The initial dataset  $\mathcal{D}_0 = [\mathbf{X}, \mathbf{y}]$ , where input  $\mathbf{X} = [\mathbf{x}^1, \dots, \mathbf{x}^{n_0}]$  with  $\mathbf{x}^i = [\ln \beta_i, 1]$ ,  $i = 1, \dots, n_0$  and  $\mathbf{y} = \ln d_o(\mathbf{u}_L)$ .
3. **Surrogate model fitting:** Fit the Bayesian GLM surrogate (Eq. (6)) to  $\mathcal{D}_t$  and obtain posterior distribution of parameters  $(a, b, \varepsilon^2) | \mathcal{D}_t$ .

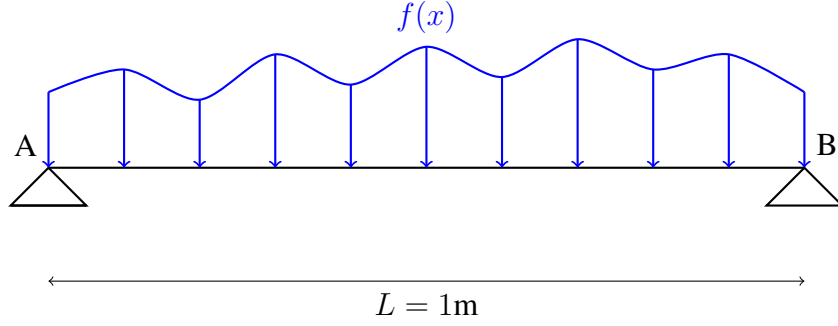


Figure 5: One-dimensional fixed-fixed static system.

4. **Posterior sampling and acquisition:** Draw  $B$  posterior samples of  $(a, b, \varepsilon^2)$  via Eq. (8). For each sample, compute the closed-form optimizer  $\beta^*$  from Eq. (12). The resulting set  $\{\beta_1^*, \dots, \beta_B^*\}$  forms the next batch of design points.
5. **Data update:** Evaluate the SROM at the new batch and augment the dataset  $\mathcal{D}_{t+1} = \mathcal{D}_t \cup \{(\mathbf{X}_j, \mathbf{y}_j) : j = 1, \dots, B\}$ .
6. **Iteration:** Repeat Steps 2–4 until a stopping criterion is reached (e.g., evaluation budget or convergence of  $\beta^*$ ).
7. **Output:** Return the final estimate  $\hat{\beta}^*$  as the nearest integer  $\beta^*$ .

## 5 Numerical example

This section compares the proposed method with the one-dimensional optimization algorithm combined with Monte Carlo sampling, using two numerical examples. All the data and code for these examples are available at <https://github.com/UQUH/SO-BO-scale>.

### 5.1 Static problem

We consider a static problem where the experimental displacement follows the model:

$$\mathbf{K}\mathbf{x}_E = \mathbf{f}_E, \quad (16)$$

with 1,000 uniformly spaced degrees of freedom (DoFs) and boundary conditions  $\mathbf{B}^\top \mathbf{x}_E = 0$  where  $\mathbf{B} = [\mathbf{e}_1 \ \mathbf{e}_n]$ . The experimental force vector is defined as:  $\mathbf{f}_E = \frac{1}{0.261466}(0.1\phi_2 + 0.4\phi_5 + 0.6\phi_8 + 2.5(\phi_{31} + \phi_{32}) - 0.015\phi_1)$ , where  $\phi_i$  is the  $i$ -th eigenvector of the stiffness matrix. The stiffness matrix is formulated as  $\mathbf{K} = \mathbf{\Phi}\mathbf{\Lambda}\mathbf{\Phi}^\top$ , where  $\mathbf{\Lambda} = \text{diag}(\lambda_i)$ ,  $\lambda_i = 4\pi^2 i^2$ ,  $i = 1, \dots, n$ . The matrix  $\mathbf{\Phi}$  is computed by the QR decomposition of matrix  $\mathbf{P}$ , where  $\mathbf{P} = \sin(k\pi \frac{j-1}{n-1})$ ,  $j = 1, \dots, n$  and  $k = 1, \dots, n$ . This setup can be interpreted as a generic one-dimensional structural system with fixed–fixed boundary conditions (see Fig. 5). In practice, the experimental model is inaccessible and is approximated by a high-dimensional model (HDM), which is defined as:

$$\mathbf{K}\mathbf{x}_H = \mathbf{f}_H, \quad (17)$$

with  $\mathbf{f}_H = \frac{1}{0.27702}(0.1\phi_2 + 0.4\phi_5 + 0.6\phi_8 + 2.5(\phi_{29} + \phi_{30} + \phi_{31}))$  and subject to the same boundary conditions. Because  $\mathbf{f}_H \neq \mathbf{f}_E$ , the HDM displacement  $\mathbf{x}_H$  deviates from  $\mathbf{x}_E$ , giving rise to model error.

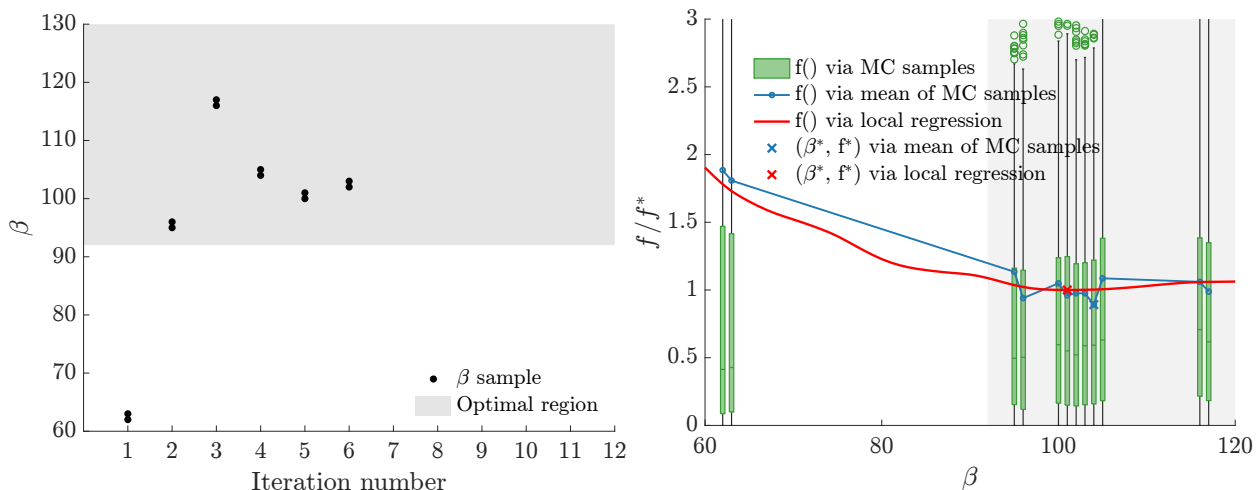


Figure 6: Static problem: progression of one-dimensional Monte-Carlo based optimization. (Left)  $\beta$  sample points during one-dimensional optimization iterations with 1000 MC samples. (Right) Objective function versus  $\beta$ , with mean trends and local regression estimates.

To efficiently characterize/correct this discrepancy, we employ the SROM framework. Firstly, a deterministic ROM is constructed by projecting the HDM onto an eight-dimensional reduced subspace spanned by the leading eight eigenvectors of  $\mathbf{K}$ . The ROM is defined as:

$$\mathbf{x}_R = \mathbf{V}\mathbf{q}, \quad \mathbf{V}^T\mathbf{K}\mathbf{V}\mathbf{q} = \mathbf{V}^T\mathbf{f}_H, \quad (18)$$

The SROM extends this construction by replacing the deterministic basis  $\mathbf{V}$  with a stochastic basis  $\mathbf{W}$ , sampled from the stochastic subspace model of [Yadav and Zhang \(2025\)](#). The stochastic subspace model has a hyperparameter  $\beta$  that controls the spread of the distribution. The goal is to estimate  $\beta$  so that the experimental validation data  $\mathbf{u}_E$  behaves like a typical SROM prediction, as formalized by the objective function in [Eq. \(14\)](#). For this example,  $d_o(\mathbf{u}_E)$  is the  $L^2$  distance between experimental and ROM displacement, and  $d_o(\mathbf{u}_L)$  is the  $L^2$  distance between ROM and SROM displacement. The hyperparameter  $\beta$  is estimated by following the methodology outlined in [Sections 3 and 4](#). The results are compared with those obtained from a one-dimensional optimization algorithm and Monte Carlo sampling.

[Figure 2](#) compares the GLM fit obtained using 290 BO samples to a GLM fit from the full dataset of 143,000 samples. Both capture the expected downward scaling trend, but the Bayesian GLM achieves this with dramatically fewer evaluations. Compared with 12,000 Monte Carlo samples for a one-dimensional optimization scheme, the Bayesian GLM requires only 290 samples to identify the optimum (see [Table 1](#) and [Fig. 6](#)). This translates into a 41-fold reduction in data usage and nearly an order-of-magnitude speedup. The improvement arises from two factors: (i) the GLM surrogate captures the expected power-law scaling, and (ii) Bayesian optimization directs sampling toward regions near the optimum, rather than expending effort uniformly across the design space.

[Figure 3](#) shows some posterior samples of  $f(\beta)$  at an iteration during the BO process, along with the corresponding Thompson samples  $(\beta^*, f^*)$ , where  $f^* := f(\beta^*)$ . We observe that optimal  $\beta$  values obtained via GLM, Bayesian GLM, and local regression all fall into the optimal region. This region is centered around the  $\beta$  estimated via local regression and is defined as the range in which the mean square error does not vary by more than 10%. As shown in [Fig. 6](#), the optimal beta obtained via the one-dimensional optimization algorithm also lies within this region. Quantitatively, the optimal

Table 1: Static problem: comparison of data and computational resources

	Bayesian GLM	1-D optimization	ratio
Data points (in numbers)	290	12,000	41.3 times
Computational time (in secs)	0.76	6	7.9 times

hyperparameter  $\beta$  is 101 using the Bayesian GLM approach, 101 using local regression, and 104 using one-dimensional optimization. Although the numerical values of  $\beta$  obtained from different approaches differ slightly, the impact on error characterization is minimal as they all fall within the optimal region.

Figure 4 illustrates the sequence of sampled points during BO iterations. The process begins with an initial set of 40 points, uniformly distributed in  $\ln \beta$ , followed by batch Thompson sampling with a batch size of 10 per iteration. The figure also shows the evolution of the posterior distribution  $\beta^*|\mathcal{D}$  and the GLM estimate. As iterations progress, the Bayesian GLM estimate converges rapidly toward the local-regression optimum. By contrast, Fig. 6 shows the sampling strategy for the one-dimensional optimization, which relies on Monte Carlo estimates using 1000 samples per  $\beta$  value—a far more data-intensive procedure.

Although the static problem is relatively simple, it clearly demonstrates the efficiency gains of the Bayesian GLM. In summary, the proposed approach achieves the same accuracy as conventional one-dimensional optimization while requiring 41 times fewer data points and delivering a 7.9-fold speedup. By concentrating evaluations near the optimum and exploiting analytic structure, the method balances accuracy and efficiency, making it particularly well-suited for complex stochastic models where brute-force Monte Carlo becomes prohibitive. To illustrate scalability and robustness, we next consider a dynamic space-structure problem.

## 5.2 Dynamics problem: space structure

We consider a dynamic problem involving a component of a space structure subjected to impulse loading in the  $z$ -direction, as illustrated in Fig. 7. The structure consists of two parts: an upper section with a heavy central mass (approximately 100 times heavier than the rest of the structure) connected to the sidewalls via rigid links, and a lower section housing essential components such as a shock absorption block. As shown in Fig. 7b, the impulse load is applied at the center of mass in the  $z$ -direction. The load propagates to the upper section through the sidewalls and to the lower section via the mounting pedestal. The functionality of critical components in the lower section may be compromised under impulse loading, making it necessary to monitor their dynamic response. The quantity of interest (QoI) is taken as the  $x$ -velocity at one of the critical nodes of the essential components. The space structure is modeled as free-floating in space, with no external boundary conditions. The dynamics of the structure are governed by a second-order ordinary differential equation (ODE) system with 42,486 DoFs:

$$\mathbf{M}\ddot{\mathbf{x}}(t) + \mathbf{C}\dot{\mathbf{x}}(t) + \mathbf{K}\mathbf{x}(t) = \mathbf{f}(t), \quad t \in [t_0, T] \quad (19)$$

with the initial conditions  $\mathbf{x}(t_0) = 0$  and  $\dot{\mathbf{x}}(t_0) = 0$ . The damping matrix  $\mathbf{C}$  is proportional to the stiffness, with a proportionality coefficient of  $6.366 \times 10^{-6}$ . The HDM is solved using the Newmark- $\beta$  time integration scheme with a time step of  $5 \times 10^{-2}$  ms. Each HDM simulation requires approximately 38 minutes of computational time, making repeated evaluations infeasible for tasks such as optimization or uncertainty quantification. To reduce cost, we construct a ROM

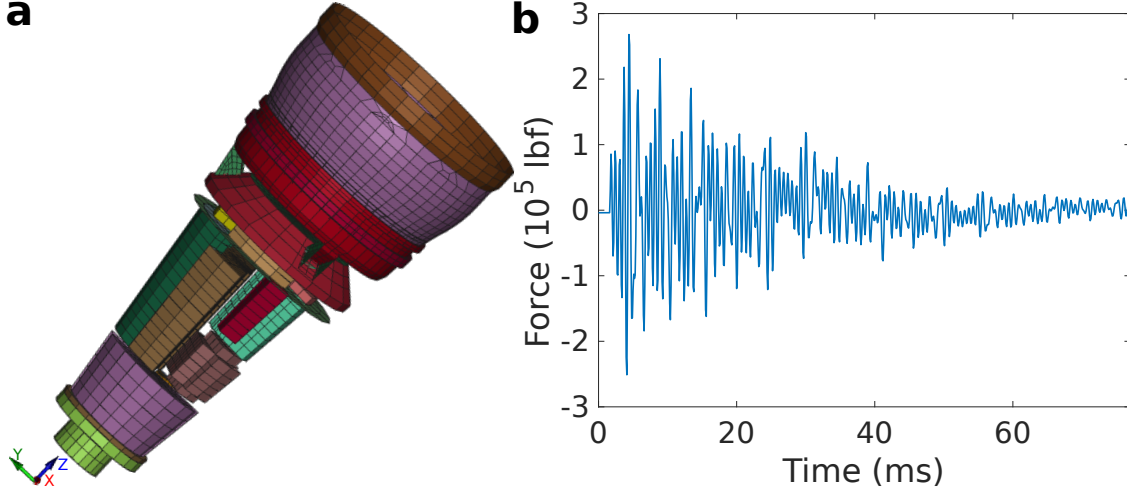


Figure 7: Dynamics problem: (a) space structure; (b) loading.

using proper orthogonal decomposition (POD) with a reduced dimension  $k = 10$ . The governing equation of the ROM is given by:

$$\mathbf{M}_k \ddot{\mathbf{q}}(t) + \mathbf{C}_k \dot{\mathbf{q}}(t) + \mathbf{K}_k \mathbf{q}(t) = \mathbf{V}^T \mathbf{f}(t), \quad \mathbf{x}_k(t) = \mathbf{V} \mathbf{q}(t), \quad t \in [t_0, T] \quad (20)$$

where,  $\mathbf{M}_k = [\mathbf{V}]^T [\mathbf{M}] [\mathbf{V}]$ ,  $\mathbf{C}_k = [\mathbf{V}]^T [\mathbf{C}] [\mathbf{V}]$ , and  $\mathbf{K}_k = [\mathbf{V}]^T [\mathbf{K}] [\mathbf{V}]$ . The ROM requires only 0.2 seconds, making it 11,200 times faster than the HDM. However, it introduces mode-truncation error, which must be characterized before practical use. We address the mode-truncation error with the SRM framework. The SRM retains the same governing form as the ROM but replaces the deterministic basis  $\mathbf{V}$  with a stochastic basis  $\mathbf{W}$  sampled from the stochastic subspace model of [Yadav and Zhang \(2025\)](#).

The hyperparameter  $\beta$  associated with the stochastic subspace model is estimated by minimizing the objective function defined in [Eq. \(14\)](#). In this example,  $d_o(\mathbf{u}_E)$  is the  $L^2$  distance between HDM and ROM velocity at a critical node, and  $d_o(\mathbf{u}_L)$  is the  $L^2$  distance between ROM and SRM velocity at the same node. We estimate the hyperparameter  $\beta$  by following the methodology discussed in [Sections 3 and 4](#) and compare the results with those obtained from a one-dimensional optimization algorithm and Monte Carlo samples.

[Figure 8](#) illustrates how the Bayesian GLM surrogate accurately captures the expected power-law scaling even from highly noisy raw data, while [Fig. 9](#) and [Fig. 10](#) show rapid convergence of the posterior distribution of  $\beta^*$ . The Bayesian GLM requires only 280 evaluations to estimate the optimal concentration parameter, compared with 13,000 evaluations for one-dimensional Monte Carlo-based optimization (see [Table 2](#) and [Fig. 11](#)). In terms of computational resources, this corresponds to a 46-fold reduction in data usage and a 40-fold reduction in runtime.

Although optimal  $\beta$  values from Bayesian GLM (40), local regression (40), and one-dimensional optimization (39) differ slightly, the impact on error characterization is minimal as they all fall into the optimal region. These results confirm that the surrogate-based strategy achieves accuracy on par with established baselines while using dramatically fewer samples.

Across both examples, the advantages of the Bayesian GLM framework are clear. Traditional one-dimensional optimization methods rely on Monte Carlo estimates at each candidate hyperparameter value, leading to noisy objectives and prohibitively high sample costs. In contrast, the Bayesian GLM constructs a surrogate that (i) exploits the expected power-law scaling with respect to the

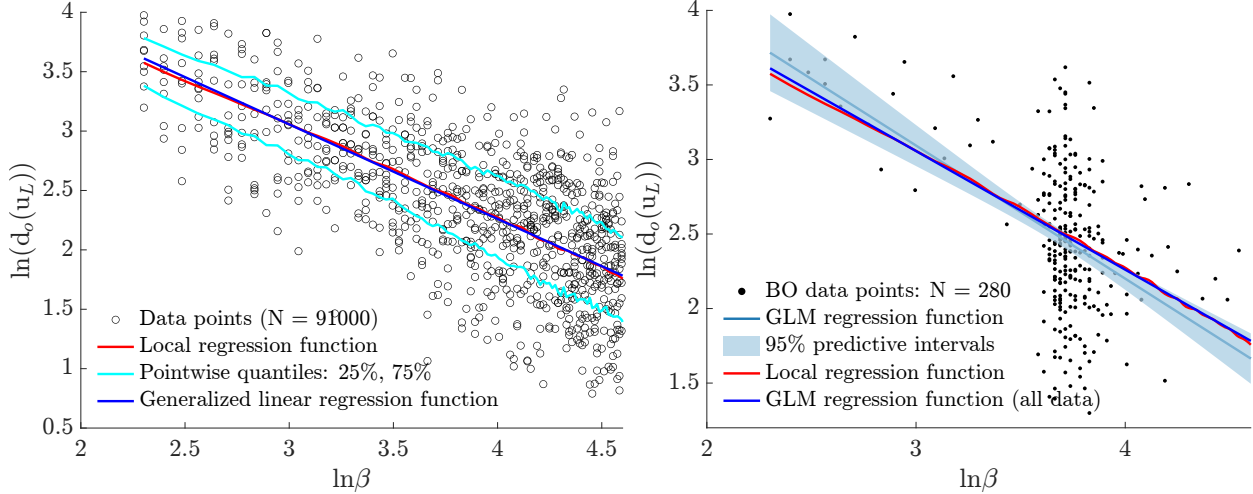


Figure 8: Dynamics problem: raw data and surrogate model fit. (Left) Raw data is highly noisy with a downward linear trend. Plotted points are 1% of the data, uniformly subsampled. (Right) Bayesian GLM captures the GLM regression function accurately with quantified error, using much fewer data points.

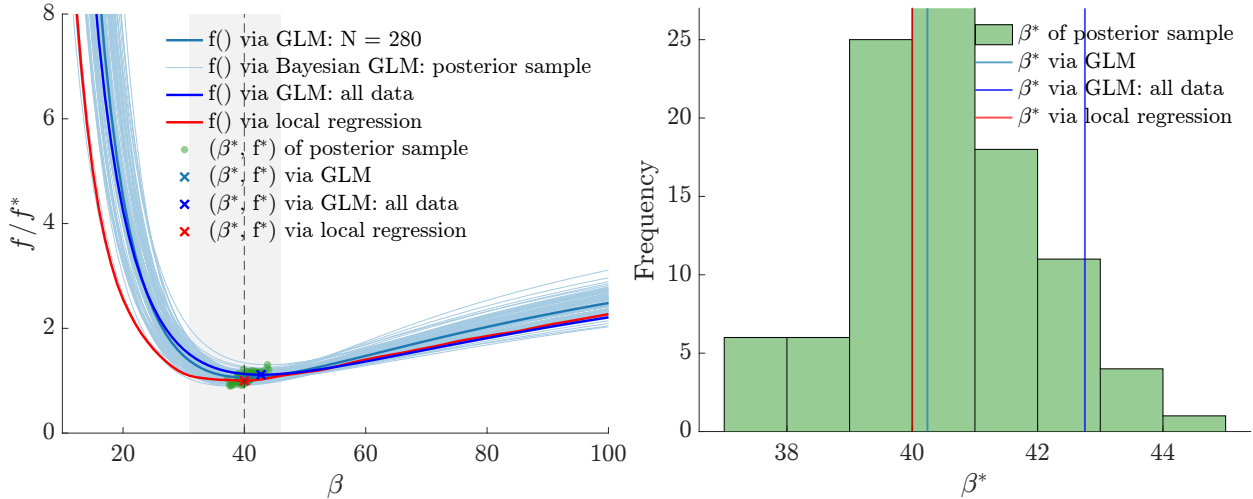


Figure 9: Dynamics problem: optimization results under different approaches. (Left) Posterior distribution of  $(\beta^*, f^*)$  well captures the true statistics. (Right) Histogram of  $\beta^*$  posterior samples.

Table 2: Dynamics problem: comparison of data and computational resources

	Bayesian GLM	1-D optimization	ratio
Data points (in numbers)	280	13,000	46.4 times
Computational time (in secs)	19.4	785	40.5 times

concentration parameter, (ii) provides an analytic evaluation of the expectation, and (iii) guides Bayesian optimization to focus sampling in the most informative regions. Across both examples, the Bayesian GLM consistently delivers accurate estimates of the optimal concentration parameter with orders-of-magnitude savings in data and runtime, establishing it as a scalable and robust tool for optimization under uncertainty.

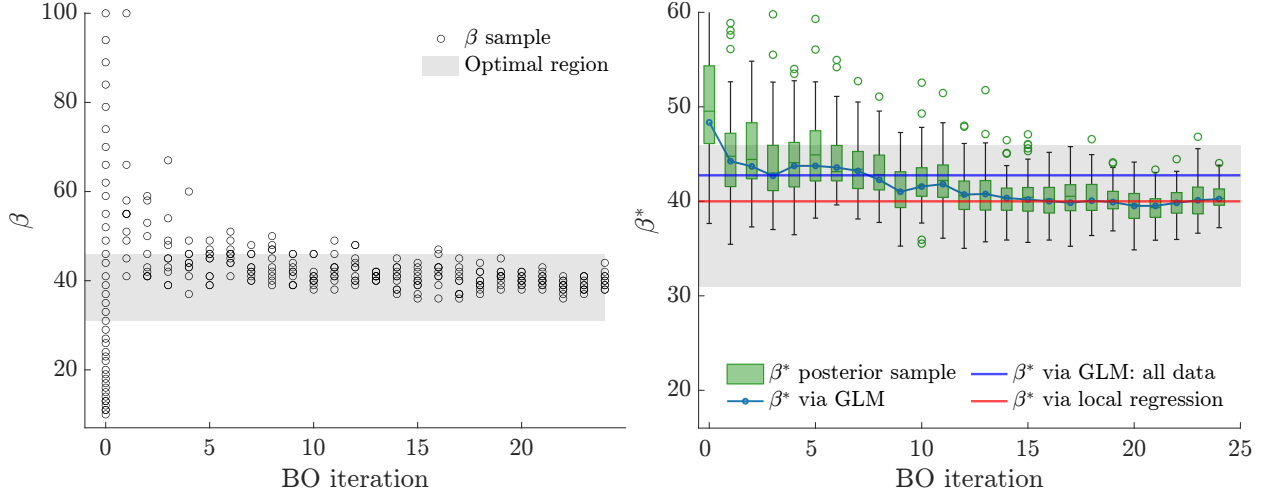


Figure 10: Dynamics problem: progression of Bayesian optimization. (Left) Sample points during BO iterations. (Right) Evolution of  $\beta^*$  posterior distribution and GLM estimate.

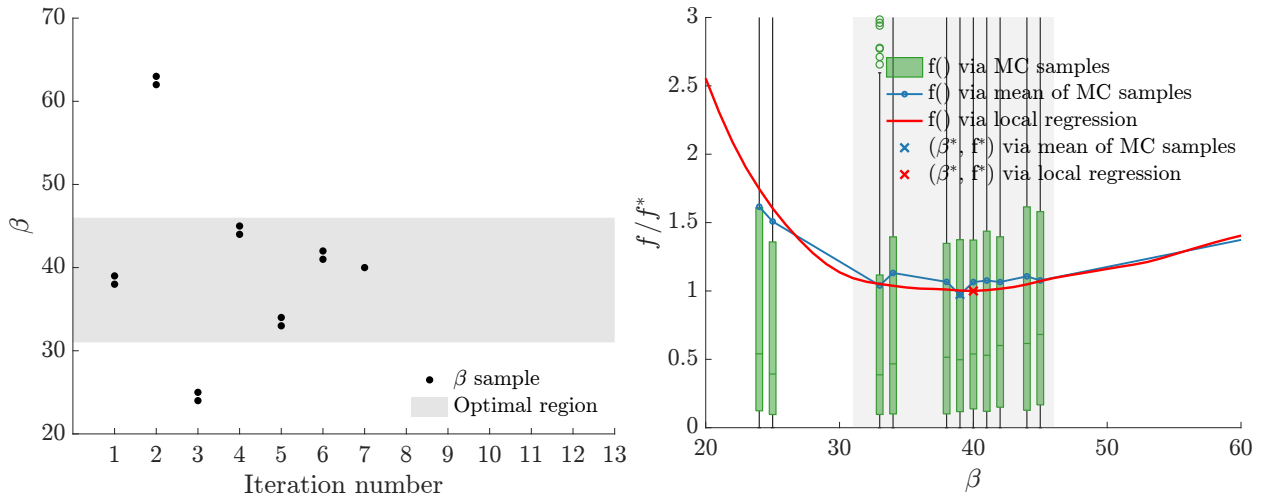


Figure 11: Dynamics problem: progression of one-dimensional Monte-Carlo based optimization. (Left)  $\beta$  sample points during one-dimensional optimization iterations with 1000 MC samples. (Right) Objective function versus  $\beta$ , with mean trends and local regression estimates

## 6 Discussion

The methodology we propose in this paper follows analytically from the surrogate model in Eq. (6), and Bayesian optimization via Thompson sampling has strong theoretical guarantees on their convergence (Russo and Van Roy, 2014). The performance of our approach therefore rests on the validity and accuracy of the surrogate model. Here we discuss these issues in detail.

The Bayesian GLM in Eq. (6) can be broken apart into three aspects: conditional mean function, conditional residual distribution, and prior on the model parameters. We validated the conditional mean model in Fig. 2 as well as in Fig. 8. Now we examine the conditional residual model, which is a stationary Gaussian white noise. To test stationarity, we compute summary statistics of the residual distributions: mean, median, standard deviation, skewness, and excess kurtosis. For each integer  $\beta$  value, 1000 sample points are used to estimate the statistics. The results for the static

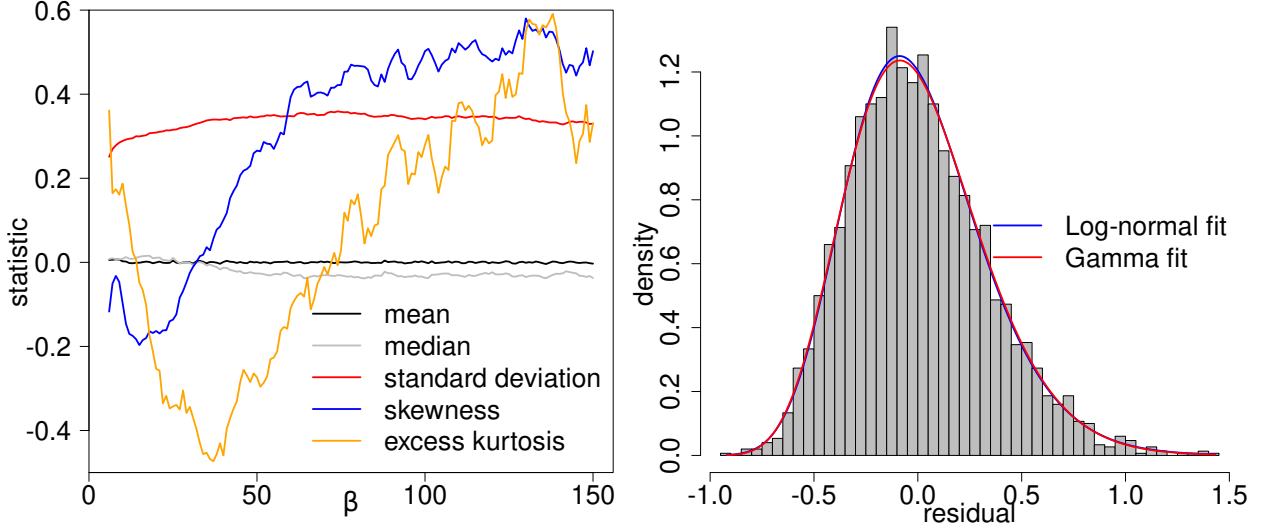


Figure 12: Diagnosis of residual distributions. (Left) Statistics of the residual distribution conditional on  $\beta$ . (Right) Histogram of the residual distribution for  $\beta = 150$ , and the best-fit PDFs using log-normal and Gamma distributions.

problem are shown in Fig. 12, smoothed with a rolling window of width 6. The sample mean of the residual, as expected, is close to zero. The median and standard deviation are largely stable for  $\beta > 50$ . A stable variance means that homoscedasticity is a valid assumption. However, skewness and kurtosis do not stabilize in the range of  $\beta$  we inspect, which means that stationarity does not hold.

To test the distributional assumption, we simply plot the histogram of the sample residual, see Fig. 12. While we assume Gaussian distribution, the motivating example in Eq. (5) points to  $\ln |z|$ , where  $z$  is a standard Gaussian random variable. On the other hand, fitting the data to classic parametric families of distributions suggests that shifted log-normal and Gamma distributions are good fits. These two distributions, however, have skewness and kurtosis tied to the log-scale and the shape parameter, respectively, making them not a robust choice across the  $\beta$  values.

Using informative priors on the model parameters can further reduce the sample size needed for an accurate surrogate model, but this requires further knowledge about the variable  $s$  and  $\beta$ . If  $\beta$  behaves like sample size and  $s$  a norm, then from Eq. (5) we may guess that the coefficient  $a$  is around  $\frac{1}{2}$  and the intercept  $\ln b$  is around  $\ln \sigma$ , and therefore impose an informative prior on  $(a, \ln b, \varepsilon^2)$  as:  $a \sim N(-\frac{1}{2}, \sigma_a^2)$  and  $\ln b \sim N(\ln \sigma, \sigma_b^2)$ . In fact, in the two examples demonstrated in the work, the estimated values of  $a$  are -0.5798 (Fig. 2) and -0.7958 (Fig. 8), respectively. However, even for the classical example, the signs and values of the parameters vary significantly based on the exact formulation of  $s$  and  $\beta$ . Imposing a strong prior thus risks steering the model in a wrong direction, undermining sample efficiency. Given that the standard noninformative prior performs well and is easy to work with, we do not pursue informative priors further in this work.

## 7 Conclusions

We have presented a novel Bayesian optimization framework tailored for optimization under uncertainty with a focus on tuning a scale- or precision-type parameter in stochastic models. The

method leveraged an inexpensive statistical surrogate to evaluate expectations analytically and enable a closed-form global solution to the optimization of the acquisition function.

Through static and dynamic structural examples, we demonstrated that the method consistently achieves order-of-magnitude gains in data and computational efficiency, reducing evaluation costs by about 40-fold compared with standard one-dimensional optimization. These results establish the proposed framework as a scalable and robust alternative for hyperparameter optimization in noisy, data-intensive settings.

While the present study focused on a single hyperparameter and assumed approximate power-law scaling, the framework can be extended to higher-dimensional parameter spaces and alternative surrogate structures. Future work will investigate these extensions and explore applications to large-scale stochastic modeling tasks in engineering, physics, and machine learning.

## Acknowledgments

This work was funded by the University of Houston through the SEED program no. 000189862.

## References

- Adebiyi, T., Do, B., and Zhang, R. (2025). “Optimizing posterior samples for Bayesian optimization via rootfinding.” *The Thirteenth International Conference on Learning Representations* (April).
- Agarwal, H. and Renaud, J. (2004). “Reliability based design optimization using response surfaces in application to multidisciplinary systems.” *Engineering Optimization*, 36(3), 291–311.
- Agarwal, H., Renaud, J., Lee, J., and Watson, L. (2004). “A unilevel method for reliability based design optimization.” *45th AIAA/ASME/ASCE/AHS/ASC Structures, Structural Dynamics & Materials Conference*, American Institute of Aeronautics and Astronautics (April).
- Andradottir, S. (1998). “A review of simulation optimization techniques.” *1998 Winter Simulation Conference. Proceedings (Cat. No.98CH36274)*, Vol. 1 of WSC-98, IEEE, 151–158.
- Azzi, M.-J., Ghnatios, C., Avery, P., and Farhat, C. (2022). “Acceleration of a physics-based machine learning approach for modeling and quantifying model-form uncertainties and performing model updating.” *Journal of Computing and Information Science in Engineering*, 23(1).
- Bai, D., Carpenter, T., and Mulvey, J. (1997). “Making a case for robust optimization models.” *Management Science*, 43(7), 895–907.
- Beland, J. J. and Nair, P. B. (2017). “Bayesian optimization under uncertainty.” *NIPS BayesOpt 2017 workshop*, Vol. 2.
- Ben-Tal, A. and Nemirovski, A. (1997). “Robust truss topology design via semidefinite programming.” *SIAM Journal on Optimization*, 7(4), 991–1016.
- Ben-Tal, A. and Nemirovski, A. (2002). “Robust optimization - methodology and applications.” *Mathematical Programming*, 92(3), 453–480.
- Bergstra, J., Bardenet, R., Bengio, Y., and Kégl, B. (2011). “Algorithms for hyper-parameter optimization.” *Advances in Neural Information Processing Systems* (December).
- Bertsimas, D., Brown, D. B., and Caramanis, C. (2011). “Theory and applications of robust optimization.” *SIAM Review*, 53(3), 464–501.

- Beyer, H.-G. and Sendhoff, B. (2007). “Robust optimization – a comprehensive survey.” *Computer Methods in Applied Mechanics and Engineering*, 196(33–34), 3190–3218.
- Birge, J. R. and Louveaux, F. (2011). *Introduction to stochastic programming*. Springer Science & Business Media.
- Carson, Y. and Maria, A. (1997). “Simulation optimization: methods and applications.” *Proceedings of the 29th conference on Winter simulation - WSC '97, WSC '97*, ACM Press, 118–126.
- Charnes, A. and Cooper, W. W. (1959). “Chance-constrained programming.” *Management Science*, 6(1), 73–79.
- Dantzig, G. B. (1955). “Linear programming under uncertainty.” *Management Science*, 1(3–4), 197–206.
- Do, B., Adebisi, T., and Zhang, R. (2024a). “Epsilon-greedy Thompson sampling to Bayesian optimization.” *Journal of Computing and Information Science in Engineering*, 24(12), 121006.
- Do, B., Ajenifuja, N. A., Adebisi, T. A., and Zhang, R. (2025). “Sampling from gaussian processes: A tutorial and applications in global sensitivity analysis and optimization.
- Do, B., Jafari Ghalekohneh, S., Adebisi, T., Zhao, B., and Zhang, R. (2024b). “Automated design of nonreciprocal thermal emitters via Bayesian optimization.” *Journal of Quantitative Spectroscopy and Radiative Transfer*.
- Do, B. and Zhang, R. (2025). “Multifidelity bayesian optimization: A review.” *AIAA Journal*, 1–37.
- Li, C. and Grossmann, I. E. (2021). “A review of stochastic programming methods for optimization of process systems under uncertainty.” *Frontiers in Chemical Engineering*, 2.
- Li, M., Mahadevan, S., Missoum, S., and Mourelatos, Z. P. (2016). “Special issue: Simulation-based design under uncertainty.” *Journal of Mechanical Design*, 138(11).
- Li, Z. and Ierapetritou, M. (2008). “Process scheduling under uncertainty: Review and challenges.” *Computers & Chemical Engineering*, 32(4–5), 715–727.
- Miller, B. L. and Wagner, H. M. (1965). “Chance constrained programming with joint constraints.” *Operations Research*, 13(6), 930–945.
- Nemirovski, A. and Shapiro, A. (2007). “Convex approximations of chance constrained programs.” *SIAM Journal on Optimization*, 17(4), 969–996.
- Oliveira, R., Ott, L., and Ramos, F. (2019). “Bayesian optimisation under uncertain inputs.” *The 22nd international conference on artificial intelligence and statistics*, PMLR, 1177–1184.
- Russo, D. J. and Van Roy, B. (2014). “Learning to optimize via posterior sampling.” *Mathematics of Operations Research*, 39(4), 1221–1243.
- Snoek, J., Larochelle, H., and Adams, R. (2012). “Practical bayesian optimization of machine learning algorithms.” *Advances in Neural Information Processing Systems 25*, Advances in Neural Information Processing Systems, 2951–2959.
- Soize, C. and Farhat, C. (2017). “A nonparametric probabilistic approach for quantifying uncertainties in low-dimensional and high-dimensional nonlinear models.” *International Journal for Numerical Methods in Engineering*, 109(6), 837–888.
- Turner, R., Eriksson, D., McCourt, M., Kiili, J., Laaksonen, E., Xu, Z., and Guyon, I. (2021). “Bayesian optimization is superior to random search for machine learning hyperparameter tuning: Analysis of the black-box optimization challenge 2020.” *Proceedings of the NeurIPS 2020*

- Competition and Demonstration Track*, Vol. 133 of *Proceedings of Machine Learning Research*, PMLR, 3–26 (06–12 Dec).
- Verderame, P. M., Elia, J. A., Li, J., and Floudas, C. A. (2010). “Planning and scheduling under uncertainty: A review across multiple sectors.” *Industrial & Engineering Chemistry Research*, 49(9), 3993–4017.
- Wang, H., Guilleminot, J., and Soize, C. (2019). “Modeling uncertainties in molecular dynamics simulations using a stochastic reduced-order basis.” *Computer Methods in Applied Mechanics and Engineering*, 354, 37–55.
- White, C., Neiswanger, W., and Savani, Y. (2021). “Bananas: Bayesian optimization with neural architectures for neural architecture search.” *Proceedings of the AAAI Conference on Artificial Intelligence*, 35(12), 10293–10301.
- Yadav, A. and Zhang, R. (2025). “Stochastic subspace via probabilistic principal component analysis for characterizing model error.” *Computational Mechanics*.
- Yang, L., Lyu, J., Lyu, W., and Chen, Z. (2023). “Efficient robust bayesian optimization for arbitrary uncertain inputs.” *Thirty-seventh Conference on Neural Information Processing Systems*.
- Zhang, R. and Alemazkour, N. (2024). “Multi-fidelity machine learning for uncertainty quantification and optimization.” *Journal of Machine Learning for Modeling and Computing*, 5(4), 77–94.
- Zhang, R. and Ghanem, R. (2020). “Demand, supply, and performance of street-hail taxi.” *IEEE Transactions on Intelligent Transportation Systems*, 21(10), 4123–4132.
- Zhang, R. and Ghanem, R. (2022). “Drivers learn city-scale intra-daily dynamic equilibrium.” *IEEE Transactions on Intelligent Transportation Systems*, 23(9), 15278–15287.
- Zhang, R., Wingo, P., Duran, R., Rose, K., Bauer, J., and Ghanem, R. (2020). “Environmental economics and uncertainty: Review and a machine learning outlook.” *Oxford Research Encyclopedia of Environmental Science*, Oxford University Press.